Data-driven Reduced Order Model for hydroacoustic analysis of ship propellers

Akash Venkateshwaran*, Ryozo Nagamune

I. ABSTRACT

In this study, we apply Dynamic Mode Decomposition (DMD) methodologies to a hydroacoustic dataset featuring a 3D marine propeller. Utilizing a meshless Lagrangian solver based on the reformulated vortex particle method (rVPM) from FLOWUnsteady, we present the hydrodynamics of propeller wake and a low-dimensional representation of the flow fields through DMD analysis.

The results illustrate DMD's capability to effectively capture spatiotemporal structures in the wake region. Moreover, a subsequent analysis post-processing acoustic signals, utilizing truncated fluid dynamic fields as input, highlights the effectiveness and precision of DMD data-driven reduced models in the prediction of propeller acoustic noises.

II. INTRODUCTION

Maritime transport has always been a major part of international commercial transportation (more than 80%), as it constitutes a highly cost-effective way of transferring large volumes of cargo between continents. As a result, there has been a dramatic upsurge in the volume of global seaborne cargo and is anticipated to increase over the coming years [1]. The increase in maritime activity has prompted detrimental consequences, including increased emissions of greenhouse gases and chemical pollutants, incidents of marine mammal collisions, and a rise in underwater noise pollution [2].

Modern ships have become the primary contributors to anthropogenic noise in the oceans responsible for increasing the ambient noise levels at low frequencies (10-1k Hz) at a rate of 3 dB/decade up until the 1980s [3]. Consequently, marine mammals pose a particular concern, given their heavy reliance on hearing for essential activities. Underwater radiated noise (URN) emitted by vessels can directly interfere with their behavior, leading to disturbances in these activities [4].

URN is influenced by factors, including vessel speed, hull shape, propulsion system, and transit conditions. Noise from a cavitating propeller outweighs other forms of propeller noise, including singing, and other hydro-acoustic noise originating from a ship [5]. The numerical simulation of cavitation and the prediction of associated noise commonly employ viscous-based Computational Fluid Dynamics (CFD) techniques such as RANS (Reynolds-averaged Navier-Stokes), DES (Detached Eddy Simulation), and LES (Large Eddy Simulation) at model scale. Within these methods, LES and DES specifically enhance the resolution of turbulent structures and cavitation dynamics, including tip vortex cavitation and the propeller URN [6]. However, LES requiring fine meshes and high timestep resolution, results in increased computational expenses. Therefore, conducting full-order simulations becomes unfeasible, particularly in scenarios involving parametric analysis and shape optimization to address URN concerns. In efforts to reduce acoustic emissions through ship design and voyage optimization, the implementation of a suitable data compression strategy that extracts the most pertinent and dominant information in a reduced-order structure is crucial for efficient data processing and quick accessibility.

To address this challenge, it is imperative to develop a Reduced Order Model (ROM) that mitigates both computational complexity and data capacity issues for real-time ship optimization problems [7]. A fundamental prerequisite for constructing an effective ROM is the assumption that the solution manifold of the underlying problem exists in a low-dimensional space, allowing expression as a linear combination of a limited number of reduced basis functions. Among the various techniques, Dynamic Mode Decomposition (DMD) has been extensively utilized owing to its versatile properties [8].

DMD has been employed in numerous studies for acoustic analysis. A DMD-based ROM was developed using hydroacoustic data derived from LES of the flow around a sphere with varying Reynolds numbers [9]. The study includes a comparative analysis of acoustic signals and spectral analysis. Additionally, DMD was applied to pressure data obtained from DES of a radial compressor, and the results were presented through modal analysis [10]. A similar investigation was carried out on the identification of acoustic modes and prediction of damping in a 3D chamber with injectors [11]. However, there is a lack of literature studies focused on developing ROMs for the hydroacoustic prediction of ship propellers.

As a result, this paper employs DMD methodologies on the wake flow field of a marine propeller to capture both spatial and temporal features and utilizes the developed model for accurate noise predictions. The structure of this paper is as follows: initially, a concise overview of the Full Order Model (FOM), acoustic model, and ROM (DMD), along with their specifications, is presented in Section. III. Section. IV provides the results of the FOM and DMD. The discussion of reconstructed and predicted flow fields along with their spectral and acoustic analysis are addressed.

Department of Mechanical Engineering,University of British Columbia, Vancouver, BC, V6T1Z4, Canada

Conclusive remarks are presented in Section. V

III. METHODOLOGY

Firstly, high-fidelity data are generated using particle based simulations. Next, the computational domain is created through the interpolation of the particle field obtained from the solver and a snapshot matrix is established. The resultant matrix of field snapshots undergoes factorization using Singular Value Decomposition (SVD), serving as the basis for constructing DMD spaces. The linear approximation of the dynamical system derived from this matrix is then employed to predict the flow field data. Subsequently, the predicted snapshots are utilized in post-processing through an acoustic analogy to validate the accuracy of noise spectral levels in comparison to the FOM data. The flow chart of the analysis conducted in this paper is shown in Fig. 1

A. Full order model

The FOM used for generating the flow field data of a marine propeller is based on the reformulated Vortex Particle Method (rVPM) implemented within the FLOWUnsteady framework [12]. FLOWUnsteady, an open-source meshless Lagrangian solver, stands out for its efficiency, using less computational resources compared to conventional CFD solvers. The output from this solver is subsequently used to compute broadband noise component using the equations formulated by Brooks, Pope, and Marcolini (BPM), while the calculation of the aeroacoustic tonal noise is carried out utilizing the Ffowcs Williams-Hawkings (FW-H) acoustic analogy [12].

VPM is a grid-independent technique for solving the vorticity-form of the Navier-Stokes equations.

$$\frac{D\omega}{Dt} = (\omega \cdot \nabla)\mathbf{u} + v\nabla^2\omega. \tag{1}$$

The approach involves discretizing the vorticity field into Lagrangian elements, referred to as vortex particles, through a radial basis function approximation involving the basis ζ_σ and coefficients Γ_p:

$$\omega(\mathbf{x}, t) \approx \sum_p \Gamma_p(t)\zeta_\sigma\left(\mathbf{x} - \mathbf{x}_p(t)\right) \tag{2}$$

Each particle consequently signifies a fluid volume carrying vorticity as it moves with the local velocity. For a more comprehensive explanation of the technique, readers are directed to reference [12]. Finally, the turbulence model for subfilter-scale (SFS) stresses related to advection and vortex stretching utilizes an anisotropic structural model that represents the phenomenon of SFS vortex stretching.

B. Hydro acoustic model

Accurate methodologies for forecasting aeroacoustic noise involve employing an acoustic analogy with the Navier-Stokes equations. One widely-used technique for calculating rotor noise is the Ffowcs Williams-Hawkings (FW-H) analogy, which simplifies the Navier-Stokes equations:

$$\bar{\Box}^2 p'(\mathbf{x}, t) = \frac{\partial}{\partial t}\left(\rho_0 \mathbf{u}_n \delta(f)\right) - \frac{\partial}{\partial x_i}\left(\Delta P_{ij}\hat{\mathbf{n}}_j\delta(f)\right), \tag{3}$$

where $\bar{\Box}^2$ represents the wave-equation operator, p' denotes the acoustic pressure, $\hat{\mathbf{n}}j$ stands for the unit normal vector pointing away from the blade surface, and $\Delta Pij = (p - p_0)\,\delta_{ij}$. The initial term on the right side is a monopole source symbolizing the volume displaced by the thickness of a solid body, the subsequent term is a dipole source portraying the force exerted on the fluid by that body, with higher-order terms (quadrupole sources) being disregarded. The tonal noise is computed using the FW-H code PSU-WOPWOP, while broadband noise is determined using the BPM method.

C. Reduced order model

Dynamic Mode Decomposition is a data-driven modal decomposition method developed in [13] for investigating the dynamics of nonlinear systems. It doesn't need complicated equations of the system; instead, it's dependent on snapshots or states of the system. DMD has the capability to recognize spatiotemporal patterns in the data which can be used to reconstruct the behavior of the nonlinear system using these repetitive patterns.

Here, we provide a concise summary of the standard algorithm. Let $\mathbf{x}_k \in \mathbb{R}^n$ denote a discrete dataset, where n represents the number of degrees of freedom or nodes, and $k \in [1, \ldots, m]$ is the time step or snapshot number. Organize the m snapshots into the data matrix $\mathbf{X} = [\mathbf{x}_1, \mathbf{x}_2, \ldots, \mathbf{x}_{m-1}]$ and its temporal evolution $\dot{\mathbf{X}} = [\mathbf{x}_2, \mathbf{x}_3, \ldots, \mathbf{x}_m]$. Seek a Koopman-like operator ($\mathbf{A}$) minimizing $||\dot{\mathbf{X}} - \mathbf{A}\mathbf{X}||_F$ for a best-fit linear approximation. This operator is given by $\mathbf{A} = \dot{\mathbf{X}}\mathbf{X}^\dagger \in \mathbb{R}^{n\times n}$, where † denotes the Moore-Penrose pseudoinverse.

The matrix $\mathbf{A}$ is not explicitly resolved (due to its n^2 elements). Instead, contemplate a reduced operator $\widetilde{\mathbf{A}}$, with significantly lower dimensionality while preserving the spectral characteristics of $\mathbf{A}$. The procedure is defined as follows:

$$\mathbf{X} = \mathbf{U}\mathbf{\Sigma}\mathbf{V}^* \approx \mathbf{U}_r\mathbf{\Sigma}_r\mathbf{V}_r^*, \tag{4}$$

where $r \leq (m-1)$ specifies the SVD truncation rank. The expressions $\mathbf{U}_r \in \mathbb{C}^{n\times r}$, $\mathbf{\Sigma}_r \in \mathbb{C}^{r\times r}$, and $\mathbf{V}_r^* \in \mathbb{C}^{r\times(m-1)}$ indicate the reduced SVD components. Subsequently, derive the reduced operator $\tilde{\mathbf{A}}$ through an $r \times r$ projection of $\mathbf{A}$ onto the modes $\mathbf{U}_r$:

$$\tilde{\mathbf{A}} = \mathbf{U}_r^*\mathbf{A}\mathbf{U}_r = \mathbf{U}_r^*\dot{\mathbf{X}}\mathbf{V}_r\mathbf{\Sigma}_r^{-1} \in \mathbb{C}^{r\times r}. \tag{5}$$

Symbolize the eigenspace of $\mathbf{A}$ as Φ (DMD modes), unveiled through the low-rank projection of the eigenvectors $\mathbf{W}$ onto the modes of $\widetilde{\mathbf{A}}$:

$$\Phi = \mathbf{U}_r\mathbf{W}, \tag{6}$$

where $\mathbf{W}$ is obtained from the eigendecomposition of $\tilde{\mathbf{A}}$:

$$\widetilde{\mathbf{A}}\mathbf{W} = \mathbf{W}\mathbf{\Lambda}, \tag{7}$$

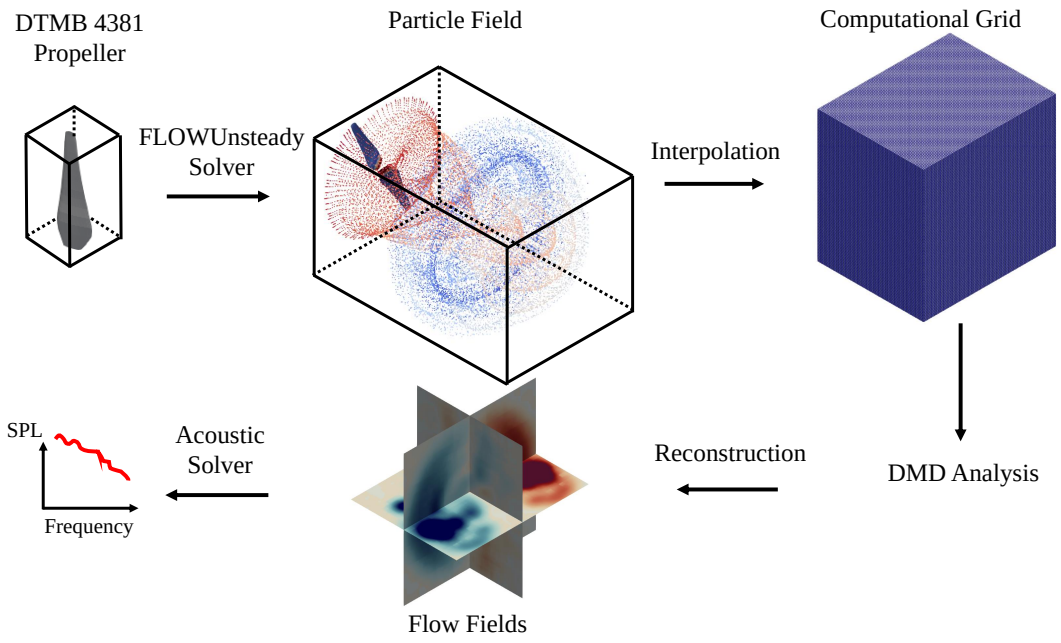

Fig. 1: Flow chart of the FOM/ROM operations performed in the present study.

and $\mathbf{\Lambda}$ is the diagonal matrix of eigenvalues of $\widetilde{\mathbf{A}}$ (also obtained from the eigendecomposition of $\mathbf{A}$). Finally, Φ and $\mathbf{\Lambda}$ provide a linear approximation to the solution vector $\mathbf{x}(t)$:

$$\mathbf{x}(t) \approx \Phi \exp(\mathbf{\Lambda} t)\Phi^{\dagger}\mathbf{x}(0). \tag{8}$$

These reconstructed fields will be used to approximate the hydroacoustic noise based on Section.III-B and compared to FOM.

D. Simulation case setup

This study involves the simulation of a right-handed marine propeller with variable pitch, no rake, and skew—specifically, the DTMB 4381 model. Detailed design specifications are available in the cited reference [14].

The propeller simulation is conducted at an RPM of 150 for a duration of 20 revolutions. The number of time steps per revolution is configured to 36, and VPM particles are released at a rate of 2 particles per step. The solver's relaxation parameters are carefully adjusted to ensure stability throughout the simulation. The convergence test is presented in the Appendix.

After computing the particle fields using FLOWUnsteady, the construction of the fluid domain surrounding the propeller is carried out for input into the DMD. This process involves interpolating the particle field quantities onto a computational grid sized $81 \times 101 \times 101$. Particularly, this interpolation is performed in the wake region of the propeller. Following this, the 3D domain is vectorized to generate a vector comprising 826,281 elements (n), representing a single snapshot. A total of 719 snapshots $(m-1)$ are used to assemble the data matrix ($\mathbf{X}$).

Acoustics are calculated with a reference pressure 1μPa (p_{ref}). The microphone to collect the pressure fluctuations is kept at a radial distance of 1m and reference angle of $-90°$. The computation is performed using 32 CPU cores in a desktop computer Intel ® Xeon ® CPU E5-2699 v3 @ 2.30 GHz.

IV. RESULTS

In this section, we present the results of FOM and ROM, accompanied by a comprehensive comparative analysis of various flow field parameters, encompassing velocity (U) and vorticity fields (W). The ROM, using truncation ranks of 10 and 20, is compared with the FOM. The tabulated representation of cumulative energy pertaining to distinct quantities at truncation ranks 10 and 20 is provided in Table. I.

Quantity	r = 10	r = 20
U_0	0.92	0.97
U_1	0.88	0.95
U_2	0.88	0.95
W_0	0.73	0.84
W_1	0.79	0.91
W_2	0.79	0.91

Table I: Cumulative energy for different quantities at truncation ranks 10 and 20.

Table. I clearly indicates that capturing the dynamics of all three components of vorticity demands a greater number of modes compared to the velocity field. Nevertheless, it is noteworthy that at r = 20, over 90% of the energy of the dynamics for all flow field quantities are successfully captured.

In the forthcoming sections, the reconstructed flow field contours are compared with FOM, and the results of the acoustic analysis are presented. Supplementary simulations

of isosurface and corresponding comparisons are available through the following drive link: Drive Link.

A. Flow field analysis

Fig. 2 and Fig. 3 show the comparative analysis of flow fields of FOM and ROM. The comparison is conducted at two key points: initially, after 3 revolutions of the propeller, and subsequently, after 20 revolutions. Flow fields are visualized across various orthogonal planes. Notably, contours in the x-y plane are omitted as they mirror those in the z-x plane due to radial symmetry. Additionally, the third component of the quantities, akin to the second component, is excluded for a concise comparison. The error fields are determined by computing the absolute differences between the ROM and FOM at each computation node and plotted alongside.

Overall, the velocity and vorticity are captured reasonably well by the ROM. Upon inspecting the error fields, it is evident that the errors are notably high during the initial stage (3 revolutions) and exhibit a substantial decrease at the later stage (20 revolutions). This is attributed to the fact that the flow field has not fully reached a steady state. Furthermore, the error field reveals that a significant portion of the error accumulates in regions with high magnitudes of the quantity. Moreover, the error field of vorticity is significantly higher than that of velocity for two reasons. Firstly, the elevated scale of vorticity potentially leads to larger errors. Secondly, capturing the dynamics of vorticity necessitates a higher number of modes, further contributing to these discrepancy.

A consistent trait observed is that DMD consistently provides a more effective reconstruction of the field on the z-y plane compared to the z-x plane across all quantities. This tendency might be attributed to the increased complexity of dynamics in the downstream direction in contrast to the transverse direction. As a result, DMD struggles to reconstruct accurate flow characteristics in the downstream direction compared to the transverse direction with the same number of modes. The results of the reconstruction substantiate that DMD can be regarded as effective tools for reducing the degrees of freedom in addressing hydro dynamic problems.

B. Acoustics analysis

The acoustic analysis undertaken in this study aims to compare the pressure fluctuation signals acquired from the FOM, as detailed in Section. III-B, with the corresponding signals obtained from DMD ROM. The signals are measured at a distance of 1m from the propeller, positioned at a reference angle of 90 degrees in the downstream direction.

Fig. 4 show the overlaid noise signals from the probe and the spectral analysis of signal. While the time series plot of the signal exhibits good agreement with the FOM noise signal, the power spectral density unveils intriguing results. The prominent peaks, located at very low frequencies, are effectively captured by the DMD signal. Specifically, with 10 modes, the spectral levels align up to a frequency of 30 Hz, while employing 20 modes extends this correspondence close to 100 Hz. Given that these low-frequency peaks encapsulate the primary and most energetic characteristics of the acoustic signal, this suggests that a moderate number of modes might serve as a favorable compromise when the acoustic analysis aims for a general characterization of the principal noise features.

V. CONCLUSION

This study examined the application of data-driven dimensionality reduction algorithms to a hydroacoustic dataset featuring a 3D marine propeller. The propeller was numerically modeled using the reformulated Vortex Particle Model within the FLOWUnsteady framework. A comprehensive dataset was presented to thoroughly assess the capacity of Dynamic Mode Decomposition (DMD) in reconstructing flow fields. The evaluation was based on their spectral and energetic contents, encompassing all spatial and temporal frequencies essential for supporting accurate predictions of noise.

The DMD model exhibited robust efficiency and precise reconstruction of both velocity and vorticity. It successfully captured a significant portion of spatial and temporal features of the field. The noise levels derived from the developed DMD model have shown notable agreement, particularly in accurately representing the high-energy components of the noise signal characterized by low frequencies.

VI. FUTURE WORK

Based on the convincing results, DMD based ROM model proves valuable for addressing ship voyage optimization problems that necessitate rapid and precise computation of noise levels for diverse propeller configurations. Furthermore, simulations of various conventional marine propellers can be conducted, introducing geometrical parameterization as an additional dimension to DMD analysis. This approach could pave the way for addressing propeller shape optimization challenges.

APPENDIX

The convergence test for the propeller simulation is monitored and presented in Fig. 5. The thrust (C_T) and torque (C_Q) coefficients are extracted from the FLOWUnsteady solver at each timestep. The simulation attains a steady state after approximately three revolutions.

REFERENCES

[1] Maxwell B. Kaplan and Susan Solomon. A coming boom in commercial shipping? The potential for rapid growth of noise from commercial ships by 2030. *Marine Policy*, 73:119–121, 2016.

[2] A review on the environmental impacts of shipping on aquatic and nearshore ecosystems. *Science of the Total Environment*, 695:133637, 2019.

[3] Chao Peng, Xinguo Zhao, and Guangxu Liu. Noise in the sea and its impacts on marine organisms. *International Journal of Environmental Research and Public Health*, 12(10):12304–12323, 2015.

[4] Christine Erbe, Sarah A. Marley, Renée P. Schoeman, Joshua N. Smith, Leah E. Trigg, and Clare Beth Embling. The Effects of Ship Noise on Marine Mammals—A Review. *Frontiers in Marine Science*, 6(October), 2019.

[5] JT Ligtelijn. Advantages of different propellers for minimising noise generation. In *Proceedings of the 3rd international ship noise and vibration conference, London, UK*, volume 26, 2007.

[6] Abolfazl Asnaghi, Urban Svennberg, and Rickard E. Bensow. Large Eddy Simulations of cavitating tip vortex flows. *Ocean Engineering*, 195(December 2017):106703, 2020.

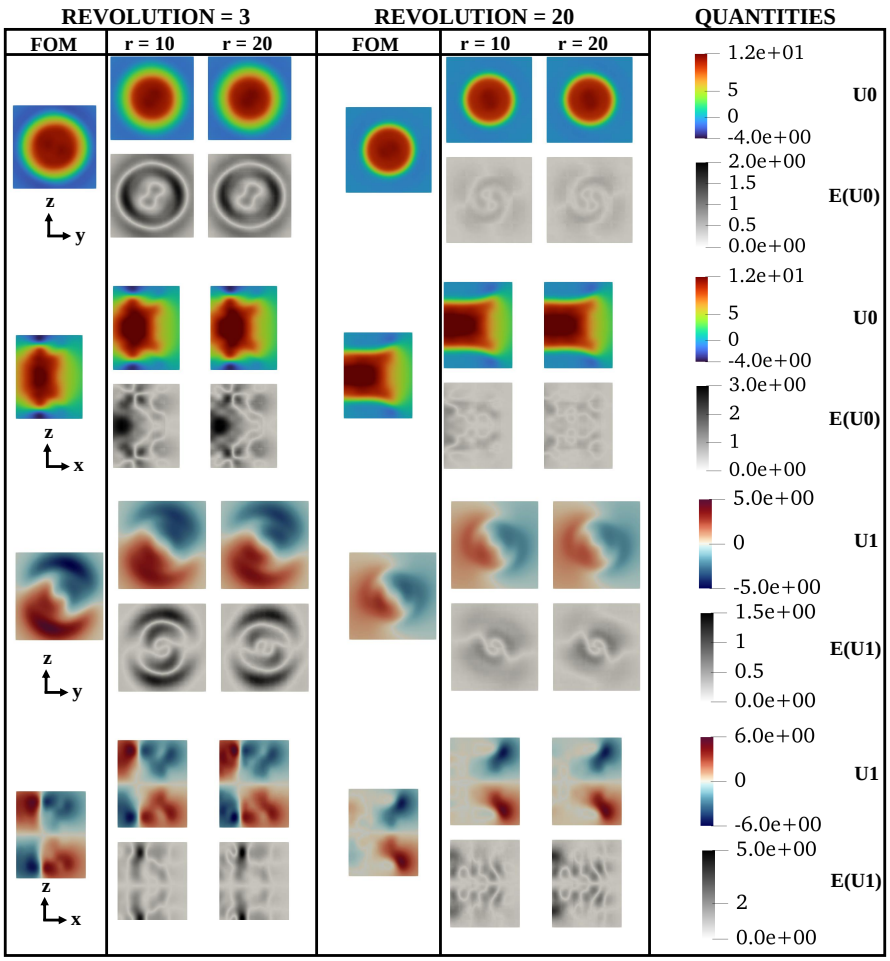

Fig. 2: Velocity contours (U), along with error fields ($E(U)$), for FOM and DMD reconstructions with r = 10 and 20. The visualization depicts the initial state at the 3rd revolution and the final state at the 20th revolution.

[7] David Amsallem, Matthew Zahr, Youngsoo Choi, and Charbel Farhat. Design optimization using hyper-reduced-order models. *Structural and Multidisciplinary Optimization*, 51(4):919–940, 2015.

[8] Soledad Le Clainche and José M. Vega. Analyzing Nonlinear Dynamics via Data-Driven Dynamic Mode Decomposition-Like Methods. *Complexity*, 2018(1), 2018.

[9] Mahmoud Gadalla, Marta Cianferra, Marco Tezzele, Giovanni Stabile, Andrea Mola, and Gianluigi Rozza. On the comparison of LES data-driven reduced order approaches for hydroacoustic analysis. *Computers and Fluids*, 216:1–36, 2021.

[10] A. Broatch, J. García-Tíscar, F. Roig, and S. Sharma. Dynamic mode decomposition of the acoustic field in radial compressors. *Aerospace Science and Technology*, 90:388–400, 2019.

[11] Guillaume Jourdain, Lars Erik Eriksson, Su Ho Kim, and Chae Hoon Sohn. Application of dynamic mode decomposition to acoustic-modes identification and damping in a 3-dimensional chamber with baffled injectors. *Journal of Sound and Vibration*, 332(18):4308–4323, 2013.

[12] Eduardo J. Alvarez, Judd Mehr, and Andrew Ning. *FLOWUnsteady: An Interactional Aerodynamics Solver for Multirotor Aircraft and Wind Energy*.

[13] PETER J. SCHMID. Dynamic mode decomposition of numerical and experimental data. *Journal of Fluid Mechanics*, 656:5–28, 2010.

[14] D. H. Bridges. A detailed study of the flowfield of a submarine propeller during a crashback maneuver. Technical Report MSSU-ASE-04-1, Department of Aerospace Engineering, Mississippi State University, 2004.

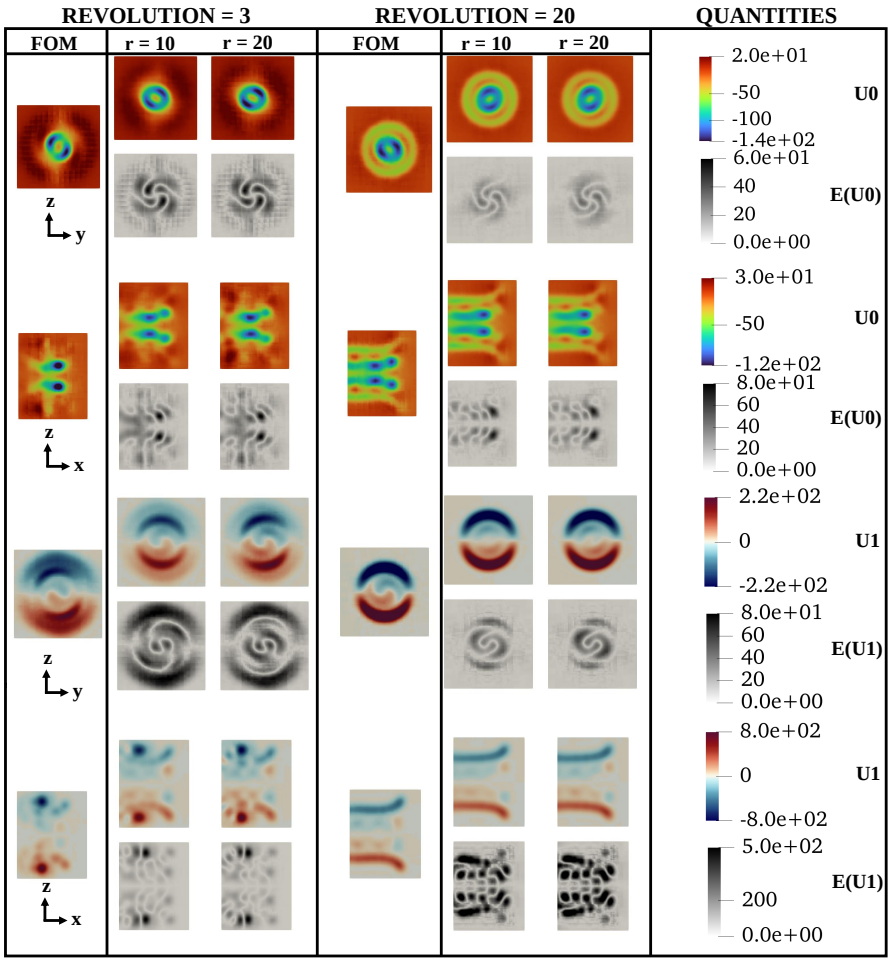

Fig. 3: Vorticity contours (W), along with error fields ($E(W)$), for FOM and DMD reconstructions with r = 10 and 20. The visualization depicts the initial state at the 3rd revolution and the final state at the 20th revolution.

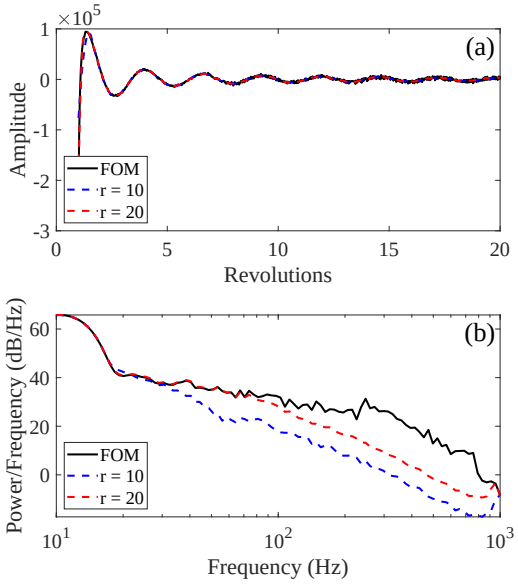

Fig. 4: Acoustics analysis: (a) Pressure fluctuation signals, and (b) Spectral analysis.

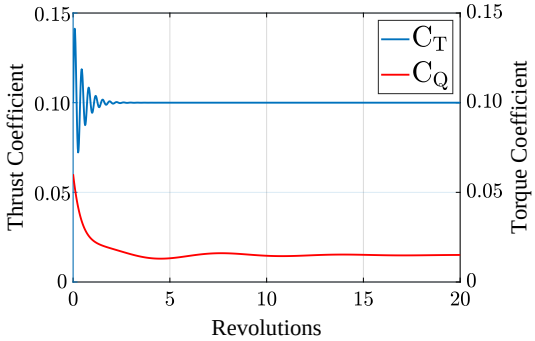

Fig. 5: Convergence of thrust and torque coefficients with respect to revolutions.